

We are IntechOpen, the world's leading publisher of Open Access books Built by scientists, for scientists

6,900

Open access books available

186,000

International authors and editors

200M

Downloads

Our authors are among the

154

Countries delivered to

TOP 1%

most cited scientists

12.2%

Contributors from top 500 universities



WEB OF SCIENCE™

Selection of our books indexed in the Book Citation Index
in Web of Science™ Core Collection (BKCI)

Interested in publishing with us?
Contact book.department@intechopen.com

Numbers displayed above are based on latest data collected.
For more information visit www.intechopen.com



Ionic Polymer-Metal Composite Artificial Muscles in Bio-Inspired Engineering Research: Underwater Propulsion

Zheng Chen, T. Um and Hilary Bart-Smith

Additional information is available at the end of the chapter

<http://dx.doi.org/10.5772/51292>

1. Introduction

Electroactive polymers (EAPs), known as artificial muscles, can generate large deflections under an electrical stimulus (Bar-Cohen 2000, 2004). Due to the similarities with biological muscles, in terms of achievable stress and strain, EAPs have great potential to be used as actuators in bio-inspired robots, bio-medical devices, and micro/nano manipulation systems. Ionic polymer-metal composites (IPMCs) are an important category of ionic EAPs (Shahinpoor & Kim, 2001, 2005; Kim & Shahinpoor, 2003, 2003; Shahinpoor et al, 2003; Kim et al, 2007; Nemat-Nasser & Li, 2000; Nemat-Nasser, 2002), which can work well under a low actuation voltage (1 to 2 Volts) in a sodium salt-water environment.

As shown in Fig. 1, an IPMC consists of one ion exchange membrane, such as Nafion (DuPont), sandwiched in between two thin metal electrodes (Shahinpoor & Kim, 2001). When the IPMC is hydrated, the positive ions in the Nafion polymer, such as sodium and calcium ions, bring water molecules and migrate to the cathode side under an electric field, whereas the negative ions are permanently fixed to the carbon chain (Nemat-Nasser & Li, 2000). The ion transportation and water migration introduce swelling in the cathode side and shrinking in the anode side, which eventually causes bending motion of the IPMC (Shahinpoor & Kim, 2001).

IPMCs can also be used for electrolysis. Electrolysis of water occurs when a relatively high voltage (> 1.6 V) is applied between the cathode and anode (Shaaban, 1994; Shimizu et al, 2005). The water molecules are decomposed into hydrogen and oxygen gases. IPMC enhanced electrolysis of water is due to several reasons; (i) ion transport brings high dense of water close to cathode side (Shahinpoor & Kim, 2001); (ii) the strong electrical fields

established on the boundary (Nemat-Nasser & Li, 2000; Nemat-Nasser, 2002) breaks down of the water molecules; and (iii) the porous platinum electrodes (Shahinpoor & Kim, 2001) on the surface acts as a stable electrolysis catalyst (Millet et al, 1989).

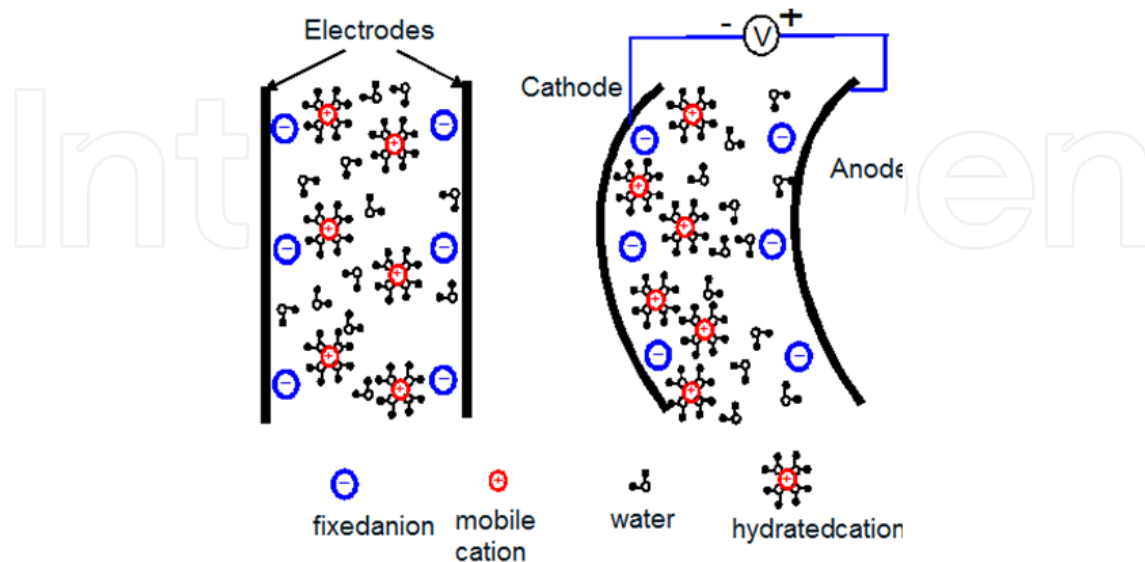


Figure 1. Actuation mechanism of IPMC (Chen & Tan, 2008).

In this chapter, the advantages and challenges of IPMCs as applied to bio-inspired engineering are discussed. A bio-inspired robotic manta ray integrated with IPMCs as artificial muscles and a novel buoyancy control device using IPMCs as an electrolysis generator are presented.

1.1. Introduction to bio-inspired robotic manta ray

Aquatic animals (e.g., fishes, cetaceans, etc.) are ultimate examples of superior swimmers as a result of millions of years of evolution, endowed with a variety of morphological and structural features for moving through water with speed, agility, and efficiency (Chen et al, 2010). The manta ray (*Manta birostris*, shown in Fig. 2) demonstrates excellent swimming capabilities; generating highly efficient thrust via flapping of dorsally flattened pectoral fins (Rosenberger, 2001). Many efforts have been directed towards building a bio-inspired pectoral fin structure to mimic the swimming behavior of the ray. Examples include rigid plates or tensegrity structures actuated by servo-motors (Gao et al, 2007; Moored et al, 2008; Moored & Bart-Smith, 2009; Zhou & Low, 2012) and flexible membrane actuated by shape memory alloy (SMA) (Wang et al, 2009). However, these methods are not suitable for small-scale robots (on the order of 5-10 cm) (Shahinpoor, 1992; Mojarrad & Shahinpoor, 1996; Tan et al, 2006; Guo et al, 2003; Punning et al, 2004) because of either the limitations in scaling or high power consumption. To construct a free swimming and small-scale robotic manta ray, there is a need for a bio-inspired actuating material that is lightweight, compliant, resilient, and capable of generating 3 dimensional (3D) deformations with portable power consumption.



Figure 2. Bio-inspiration: The Manta Ray (courtesy of www.elasmodivec.com).

In the past, IPMC actuators have been used as a caudal fin in bio-inspired robotic fishes (Shahinpoor, 1992; Mojarrad & Shahinpoor, 1996; Tan et al, 2006; Guo et al, 2003), where the propulsive fin mimics the bending motion observed in many biological fishes. In the propulsion mechanism of rays, undulatory and oscillatory flapping motions of the pectoral fin play an important role in generating highly efficient propulsion and maneuvering (Rosenberger, 2001). To fabricate an actuating membrane capable of generating complex deformations, lithography-based (Chen & Tan, 2010) and surface machining-based approaches (Kim et al, 2011) have been explored to pattern the electrodes of the IPMC. To create active and passive areas in a Nafion membrane, the electrodes on the membrane were separated. By independently controlling the bending of each active area, 3-dimensional deformations of the membrane have been achieved. However, the stiffness of the Nafion in the passive area limited its capability of generating large twisting motions. Punning et al, developed pectoral fins for ray-like underwater robot by assembling separated IPMC beams with a latex foil (Punning et al, 2004). However, this robot did not achieve free-swimming due to high power consumption and low propulsion efficiency. The challenge in this study is to fabricate a compliant actuating membrane capable of complex 3D kinematic motions capable of generating energy efficient locomotion. This will then be integrated in a small-scale robotic ray capable of free swimming.

1.2. Introduction to bio-inspired depth control device

A simple and efficient method for buoyancy control is critical in the design of an autonomous underwater device. The most common method used today to achieve depth control is to utilize a piston-cylinder assembly connected to a servomotor (Lin et al, 2010). A cylinder, usually containing air, is compressed and expanded to adjust the volume of the system. Another similar approach is to use a water-pump powered bladder to compress the air in a blaster tank (Zhou & Low, 2012). These two methods usually yield reliable results with relatively fast response times. However, in addition to the significant noise generated by the servomotors, there are limitations in scaling the servomotor. Consequently, this

solution is not feasible for implementation in small devices. In order to build more efficient buoyancy control devices, researchers have turned to biology for inspiration for the next generation of autonomous underwater vehicles.

Biology has many novel and effective depth control mechanisms suitable for a variety of environments. For example, sperm whales (Fig. 3(a)) achieve buoyancy control by using their spermaceti oil. An adult sperm whale contains about 4 tons of spermaceti oils in their spermaceti organ, which represents approximately 8% of its total mass (Shibuya et al, 2006). The spermaceti oil has a low melting point and its density depends largely on the temperature of the oil. By manipulating the arterial blood flow through the spermaceti organ, the sperm whales can regulate the temperature of the oil and are thus able to control their buoyancy. There have been recent demonstrations of buoyancy control concepts manipulating temperature to change the density of oil (Shibuya et al, 2006) or wax (McFarland et al, 2003). However, the response times are slow (on the order of 10 minutes), and it is inefficient for small devices because a constant power must be supplied to maintain the temperature of the oil while cruising at a certain depth. Ray-finned fishes, such as one depicted in Fig. 3(b), change the buoyancy of their body using a swim bladder (Bond, 1996). Expansion of the bladder results in increased volume, thus making the body more positively buoyant and vice versa. Inspiration for the artificial bladder presented in this chapter comes from these ray-finned fishes. The challenges arise from how to generate and release the gas to control the volume of the bladder underwater.

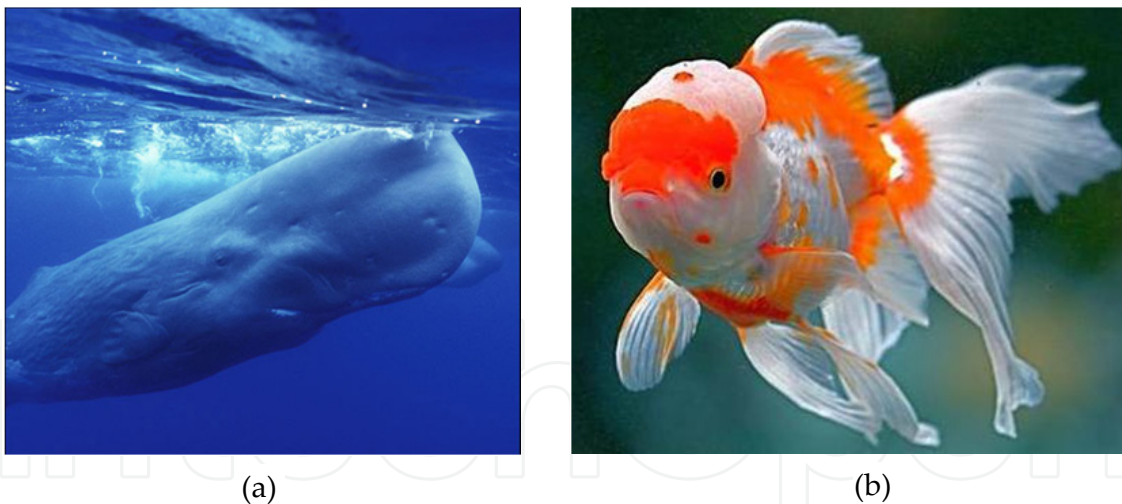


Figure 3. (a) Sperm whale (*Physeter macrocephalus*); (b) Golden fish (*Carassius auratus*).

The rest of this Chapter is organized as the follows. Section 2 is focused on the development of a bio-inspired robotic manta ray powered by IPMC artificial pectoral fin. Fabrication and characterization of the artificial pectoral fin and design of the robotic manta ray are presented. Section 3 is focused on bio-inspired depth control device enabled by IPMC enhanced water electrolysis, where the buoyancy control mechanism, device design, and open loop testing are demonstrated. Conclusions and future work on both studies are discussed in Section 4.

2. Bio-inspired robotic manta ray powered by IPMC artificial pectoral fin

In this section, we present a bio-inspired, free-swimming robotic manta ray propelled by artificial pectoral fins. In our previous work, we developed an assembly-based fabrication process to bond four IPMC actuators with Polydimethylsiloxane (PDMS) elastomer to create an actuating membrane capable of 3D kinematic motions (Chen et al, 2011). However, the control strategy for four IPMCs is too complicated to be implemented on-board. In this study, a pectoral fin, with the planform shape of a manta ray pectoral fin and consisting of one IPMC artificial muscle in the leading edge and a passive PDMS membrane in the trailing edge, has been designed. When the IPMC is actuated, the passive PDMS membrane follows the bending of IPMC with a phase delay, which causes an undulatory motion of the fin. The pectoral fin has been characterized by key factors as they relate to the function of the robot: tip deflection; twist angle; and power consumption. Since only one IPMC is needed for actuation in the pectoral fin, the control strategy is greatly simplified. To test the performance with a free-swimming robot, a light, compact on-board control unit with a lithium ion polymer battery has been developed. Experimental results have shown that the robot is capable of free swimming.

2.1. Fabrication of artificial pectoral fin

The proposed artificial pectoral fin must be able to generate oscillatory motion with a twist angle as observed in swimming of the manta ray, under hydrodynamic loads. An artificial pectoral fin was fabricated by combining one IPMC actuator with a PDMS elastomer in a mold to create a predefined planform shape. The design of pectoral fin is shown in Fig. 4(a). The outline shape of the fin mimics that of the manta ray. The fin is divided into two areas: IPMC beam on the leading edge and PDMS passive membrane on the trailing edge. Note that the size and shape of the IPMC is chosen to generate enough bending moment with limited power consumption. Optimal design of the fin will be focused in the future work.

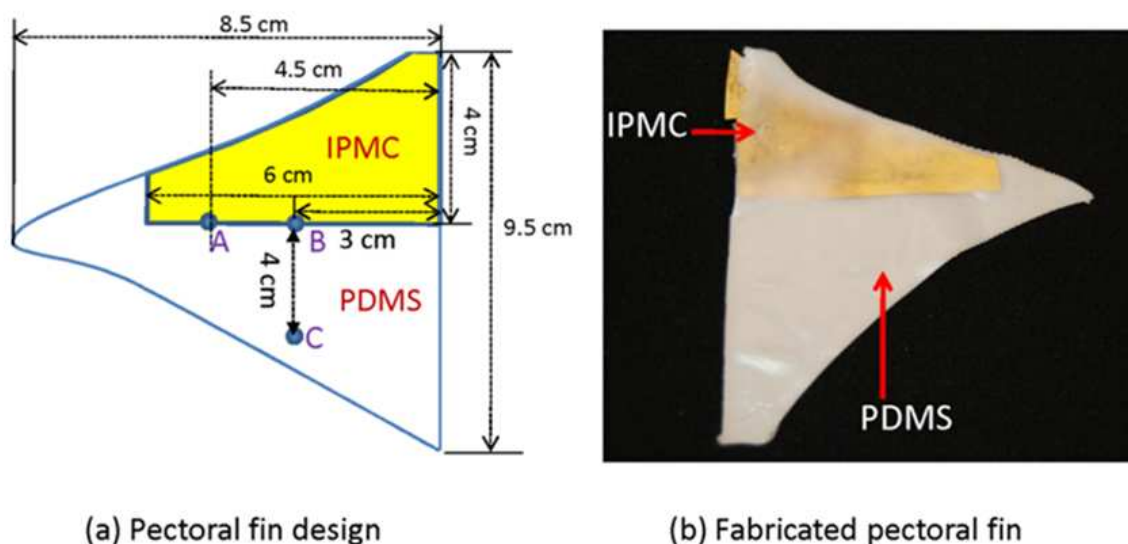


Figure 4. IPMC powered artificial pectoral fin.

The first step in creating the artificial pectoral fin is to fabricate the IPMC actuator. Many groups have developed different IPMC fabrication processes for various purposes (Kim & Shahinpoor, 2003; Chung et al, 2006; Lee et al, 2006; Kim & Shahinpoor, 2002). In our fabrication method, we followed most of the procedure outlined by K. Kim and M. Shahinpoor (Kim & Shahinpoor, 2003) but added additional platinum/gold plating process to reduce the surface resistance of the electrodes (Lee et al, 2006). The following supplies are used to fabricate the IPMC beams: (1) Nafion ion exchange membrane Nafion 1110 (258 μm thick, DuPont); (2) tetraammineplatinum chloride 98% (Aldrich); (3) sodium borohydride (NaBH_4 , Aldrich); (4) dilute ammonium hydroxide solution (NH_4OH 29% solution); (5) dilute hydrochloric acid (HCl aq, 1.0 N solution); and (6) de-ionized water. Fig. 5 shows the IPMC fabrication process. The major fabrication steps are as follows:

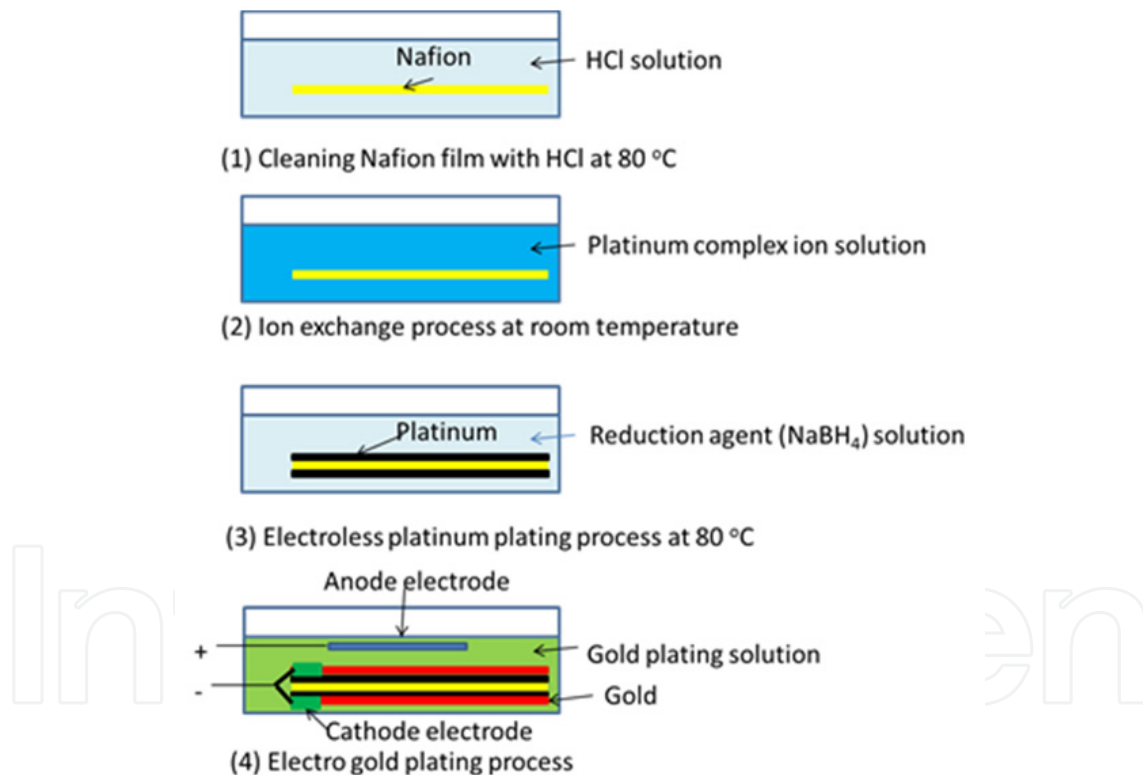


Figure 5. IPMC fabrication process.

1. Treatment of Nafion with HCl (cleaning). This step is to remove metal particles and other impurities from the film. The Nafion film (10 cm by 5 cm) is boiled in 1.0 N hydrochloric acid (HCl) at 80 °C for 30 min. The film is then rinsed with DI water to remove acid residue.

2. Ion exchange process. The purpose of the ion exchange process is to enable the Nafion film to absorb enough platinum complex ions $\text{Pt}(\text{NH}_4)_2^{2+}$, which will be reduced to platinum particles to form electrodes in step 3. The membrane is then immersed in 50 ml tetraammineplatinum Chloride hydrate solution (3 mg/ml) mixed with 1 ml ammonium hydroxide (29%) to make a weak base environment. The ion exchange process takes about 3 hours to allow the Nafion film to fully absorb enough platinum complex ions.
3. Electroless platinum plating. In this step, the platinum complex ions are reduced to platinum particles to create the metal electrodes on the outer surfaces of the Nafion film. The ion-exchanged Nafion film is placed in a DI water bath. Then the bath is gradually heated to 40 °C. A sodium boron hydride solution (NaBH_4) (20 mg/ml) is prepared, which is used as a reducing agent. 5 ml NaBH_4 solution is added to the bath and the temperature of the bath is increased to 65 °C. 5 ml NaBH_4 solution is added to the bath every 30 min. After 3 h plating, approximately 6 μm of platinum is deposited on the surface with good polymer-metal adhesion.
4. Electro gold plating: To further improve the conductance of the electrode, about 1 μm thick gold was deposited on the surface via electroplating process. The sample was then submerged in a sodium solution (1 N) for one day to exchange H^+ with Na^+ to enhance the actuation performance of the IPMC.

After fabrication of the IPMC actuator, the next step is to bond the IPMC with a PDMS elastomer membrane. The PDMS bonding process (shown in Fig. 6) is described in the following 5 steps. (1) A Delrin polymer (McMaster) mold was made using a Computer Numerical Control (CNC) rapid milling machine (MDX-650, Roland). The mold has two concaved areas to house the PDMS passive membrane and IPMC actuator. The thicknesses of PDMS membrane and IPMC are 600 μm and 280 μm , respectively. (2) The IPMC was cut into the shape shown in Fig. 3(a). (3) About 3% glass bubbles (Glass bubble K37, 3M Inc) were added into PDMS gel (Ecoflex 0030, Smooth-on Inc.) to gain a neutrally buoyant pectoral fin. (4) The IPMC and the PDMS gel were then clamped with the mold and the PDMS was cured at room temperature for 3 hours. (5) The IPMC/PDMS artificial pectoral fin (shown in Fig. 4(b)) was removed from the mold. Note that there is about 150 μm thick PDMS covered on the top of IPMC to guarantee good bonding between passive and active areas. The additional layer of PDMS stiffens the IPMC active area. However, since the PDMS (Ecoflex) is an extremely compliant material (Young's modulus, 0.06 MPa), compared to the Nafion (Young's modulus 114 MPa), the stiffening effect can be neglected.

2.2. Characterization of pectoral fin

The pectoral fin was characterized in terms of tip deflection, twist angle, and power consumption. These characteristics are useful in providing comparison data in the design of the bio-inspired robot. To characterize the actuating response of the pectoral fin, three testing points (A, B, C) are defined on the membrane (shown in Fig. 4(a)).

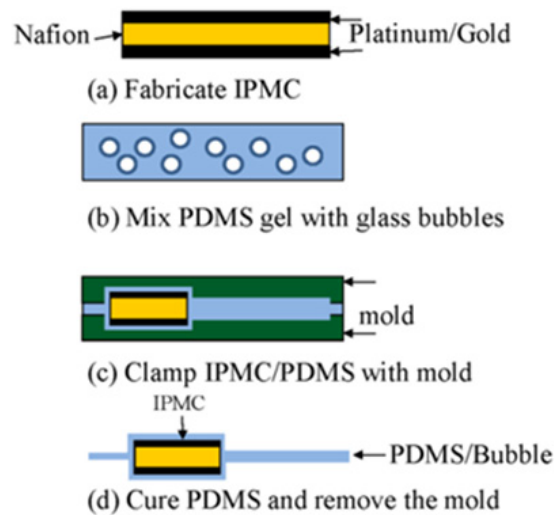


Figure 6. Fabrication process of pectoral fin.

2.2.1. Tip displacement

To measure the tip deflection, the fin was actuated in a transparent tank containing water. A laser sensor (OADM 20I6441/S14F, Baumer Electric) was fixed outside of the tank to measure the bending displacement at point A. Note that due to large deflection of the fin, the laser sensor was unable to capture the bending displacement of the tip. So we moved the measurement point from the tip to the point A. The tip deflection was normalized by dividing the bending displacement by the length at the point A. Fig. 7 shows the tip deflection when a square wave actuation voltage (0.09 Hz, 4 V) was applied to the IPMC. It shows a peak-to-peak deflection of 100% in the span-wise direction. One can achieve a larger deflection by applying a higher actuation voltage. But there is a limit to the size of voltage applied across the IPMC—anything greater than 6 V risks dielectric breakdown through the IPMC (Lee et al, 2006).

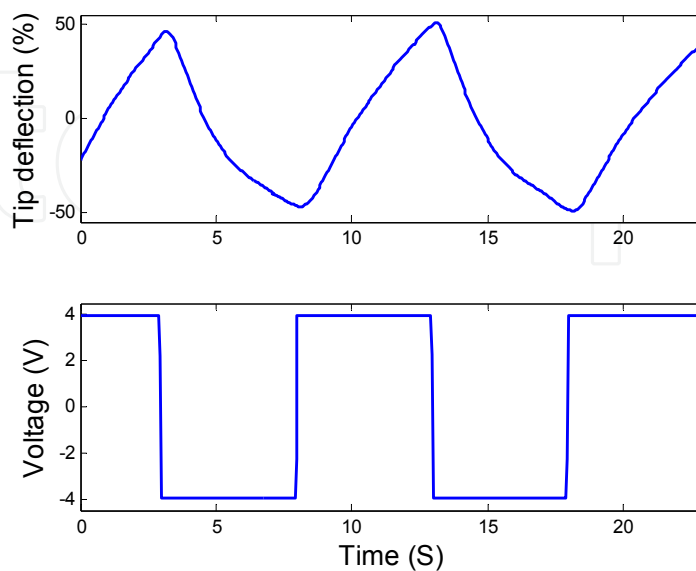


Figure 7. Tip deflection of the pectoral fin.

2.2.2. Bode plot

To capture the Bode plot of the pectoral fin, a series of sinusoidal actuation signals with amplitude of 4 V and frequencies ranging from 0.05 Hz to 0.9 Hz were applied to the IPMC. The tip deflection at the point B and the actuation voltage were measured. The magnitude and phase shift of the tip deflection over the actuation voltage were calculated. The Bode plot (Fig. 8) demonstrates that the actuation dynamics of the pectoral fin behaves as a low-pass filter with a 0.4 Hz cut-off frequency. This is to be expected as the ions in the IPMC cannot move very rapidly (Nemat-Nasser, 2002) and hydrodynamic force dumps high frequency vibration (Chen & Tan, 2010).

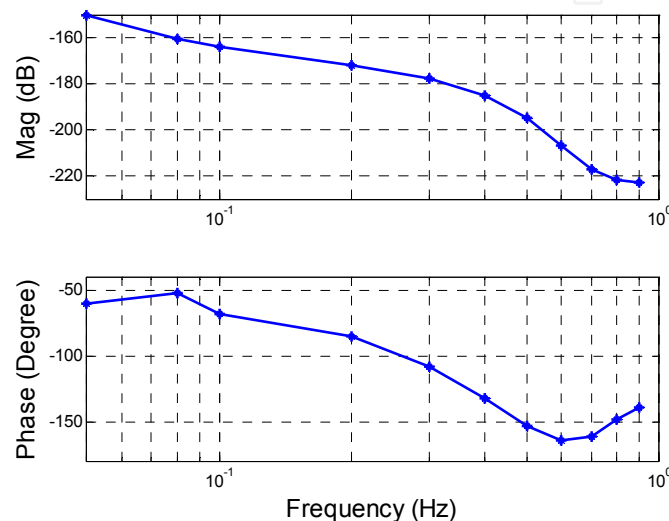


Figure 8. Bode plot of pectoral fin.

2.2.3. Characterization of twisting motion

In order to characterize the 3-dimensional (3D) kinematics of the fin, two laser sensors (OADM 20I6441/S14F, Baumer Electric) were used to measure the bending displacements at the points B and C, d_B and d_C respectively. The twist angle was calculated by

$$\alpha = \tan^{-1} \left(\frac{d_B - d_C}{BC} \right) \quad (1)$$

where $BC=20$ mm.

A series of square wave voltage signals were generated via LabVIEW (National Instruments), amplified using power amplifiers, and then applied to the IPMC actuator. All signals have the same amplitude of 4 V but varying frequencies from 0.06 Hz to 1 Hz. As the IPMC actuator is being used to generate thrust in underwater vehicles, the 3D kinematics was quantified in water. The fin was placed in a water tank and the laser sensors were fixed outside of the tank. Fig. 9 shows the twisting and flapping motion on the fin at $f=0.09$ Hz. The upper figure shows the bending displacements d_B and d_C , which indicates a phase delay

and an amplified magnitude between the bending motions at the points B and C. The lower figure shows the calculated twist angle. The peak-to-peak twist angle is 40° . Fig. 10 shows the plot of twist angle versus operating frequency. The twist angle decreases as the frequency increases. The cut-off frequency of twist angle is around 0.1 Hz. Since the twist angle plays an important role in generating a thrust, the optimal operating frequency of the robot will be set around 0.1 Hz.

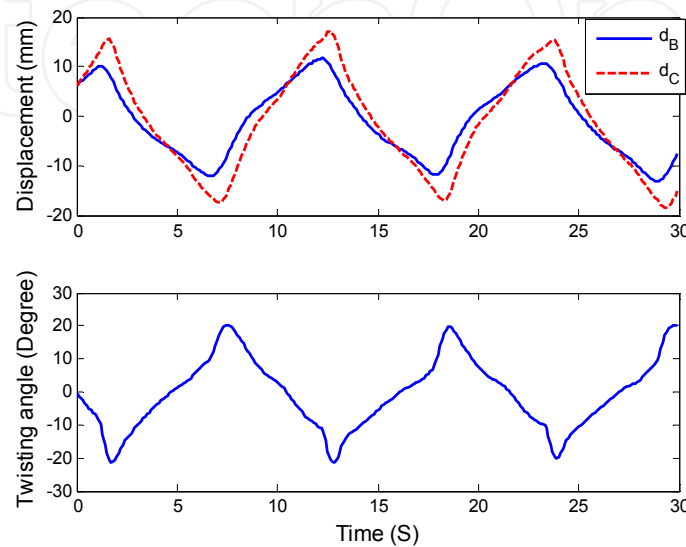


Figure 9. Twisted flapping motion on the fin.

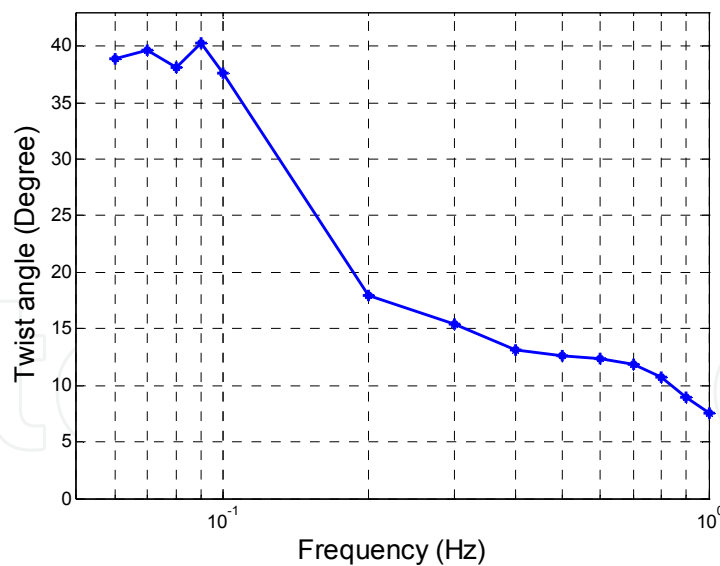


Figure 10. Twist angle versus operating frequency.

2.2.4. Power consumption

For un-tethered bio-inspired robot applications, key questions regarding power consumption and optimal power management must be addressed. In this section, we study the power consumption of the pectoral fin under a square wave actuation voltage, which is

easy to generate on board. The power consumed by the IPMC was calculated using the following equation:

$$P = \frac{1}{T} \int_0^T i(t)v(t)dt \quad (2)$$

where $i(t)$, $v(t)$, and T are measured actuation current, voltage, and period, respectively. A 4 V, 0.1 Hz square wave voltage was applied to the IPMC of the pectoral fin, which was fixed under water. Fig. 11 shows the actuation voltage and current. The power consumption at 0.1 Hz is 1.09 W.

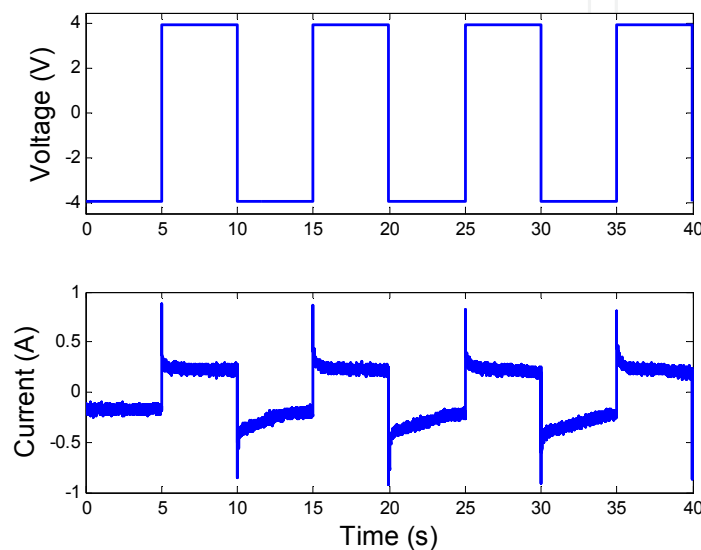


Figure 11. Actuation current and voltage under a 0.1 Hz square wave signal.

Under an electrical voltage signal, the IPMC behaves as a pseudo capacitor. When the applied voltage changes its polarization, the current reaches its peak, and then drops down to a steady-state current. The steady-state current is due to the DC resistance of the polymer and the water electrolysis on the electrodes. To reduce the power consumption of the pectoral fin, it would be better to eliminate the water electrolysis by coating a waterproof protecting layer on the IPMC, which will be our future focus. To study the relationship between power consumption and operating frequency, a series of square wave actuation signals with amplitude of 4 V and frequencies ranging from 0.1 Hz to 1 Hz were applied to the fin. Fig. 12 shows the power consumption versus operating frequency. It demonstrates that they are positively related and the power consumption is below 1.5 W.

2.3. Design of robotic manta ray

In our previous work, a free swimming and IPMC enabled robotic manta ray was developed for the first time (Chen et al, 2011). We used four IPMC beams bonded with thin PDMS membrane to create artificial pectoral fin. By independently controlling the bending of each IPMC beam, the fin can generate undulatory motions. However, in the free-swimming test of the robot, only a flapping motion was generated due to the complexity of generating the

four control signals on-board. In this paper, we present an IPMC-enabled robotic manta ray capable of free swimming. Since there is only one IPMC beam in the leading edge, a single signal is generated on-board, greatly simplifying the control strategy.

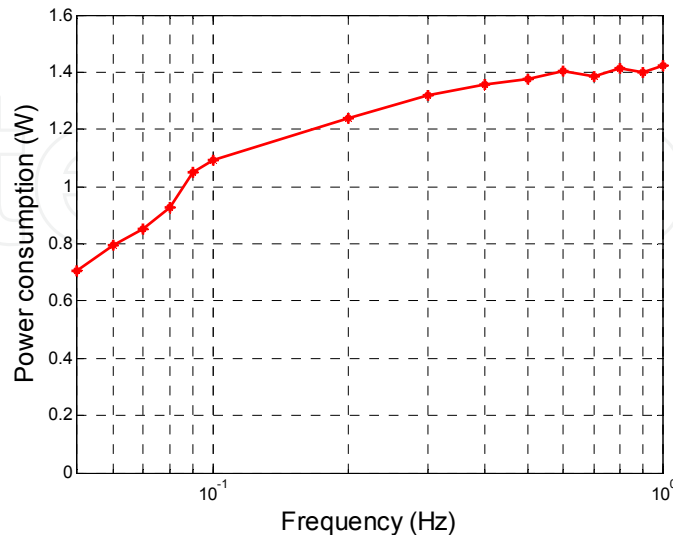


Figure 12. Power consumption versus operating frequency.

2.3.1. Control circuit

The on-board circuit, which was developed in our previous work (Chen et al, 2011), provided a square wave voltage signal to the IPMC actuator in the pectoral fin. Fig. 13(a) shows the schematic of the circuit. A 555-timer was used to generate a frequency adjustable square wave. The amplitude of the voltage signal, V_p , was controlled by an adjustable voltage regulator. An H-bridge driver was used to draw up to 2 A output peak current. A rechargeable 7.3 V Lithium Ion Polymer battery (400 mAh, AA Portable Power Corp) was selected as the power source for the robot. Fig. 13(b) shows the picture of PCB board and battery.

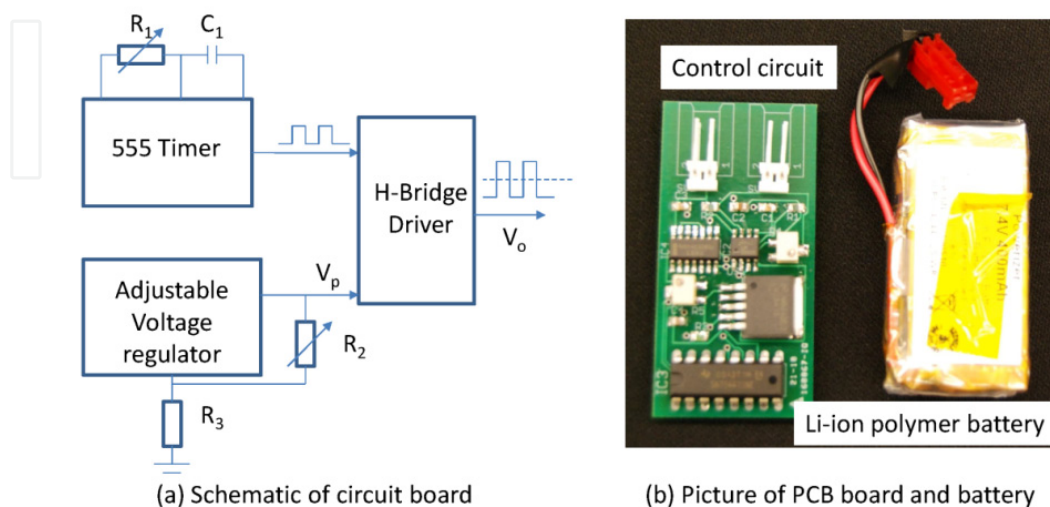


Figure 13. Control circuit and battery (Chen et al, 2011).

2.3.2. Free swimming robot design

Fig. 14 shows the overall shape of the robot. Two acrylic frames with gold electrodes were made to clamp the artificial wings to the body support. Gold electrodes were used to minimize corrosion. Polymer foam was put into the middle of the frame to make the robot slightly positively buoyant. A simple hinged plastic box was used to house the circuit board and battery. Once closed, only two wires were exposed outside the box. PDMS was used to seal the box waterproof. The plastic box was then glued on the top of the robot. With the robot was put under the water, the cover of the box was above the water level thus water could not leak into the box. The fully assembled robot was 11 cm long, 21 cm wide, and 2.5 cm thick with a mass of 55 grams. The free-swimming robot with the control unit is shown in Fig. 15. The total cost of the robot is about \$200.

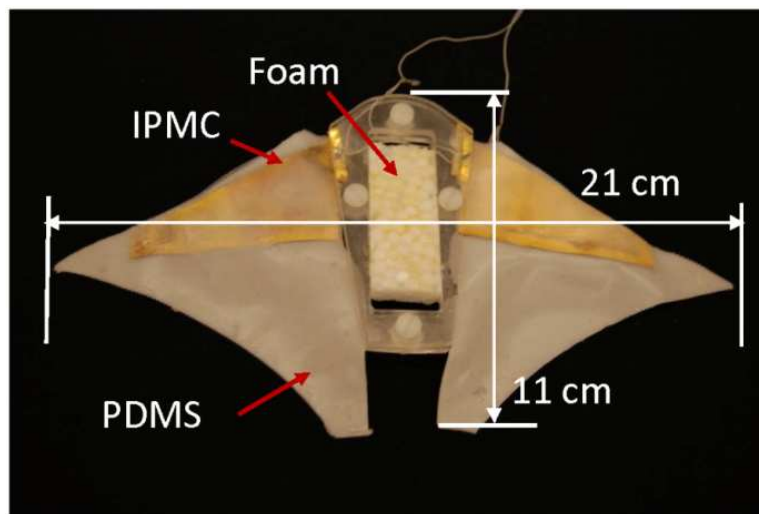


Figure 14. Robotic manta ray body.



Figure 15. Free swimming robotic manta ray body.

2.3.3. Free-swimming test

The robot was tested in a water tank (1.5 m wide, 4.7 m long, and 0.9 m deep). The robot was positively buoyant. The operating frequency of the square wave actuation voltage was tuned to 0.167 Hz and the amplitude was set to 4 V. Since each pectoral fin consumed less than 1.2 W (shown in Fig. 11), the overall power consumption of the robot was under 2.5 W. A digital video camera (VIXIA HG21, Canon) was used to capture the motion of the swimming robot. Fig. 16 presents six snap shots of the swimming robot from top view, where the trajectories of left and right fins are plotted in blue and red, respectively.

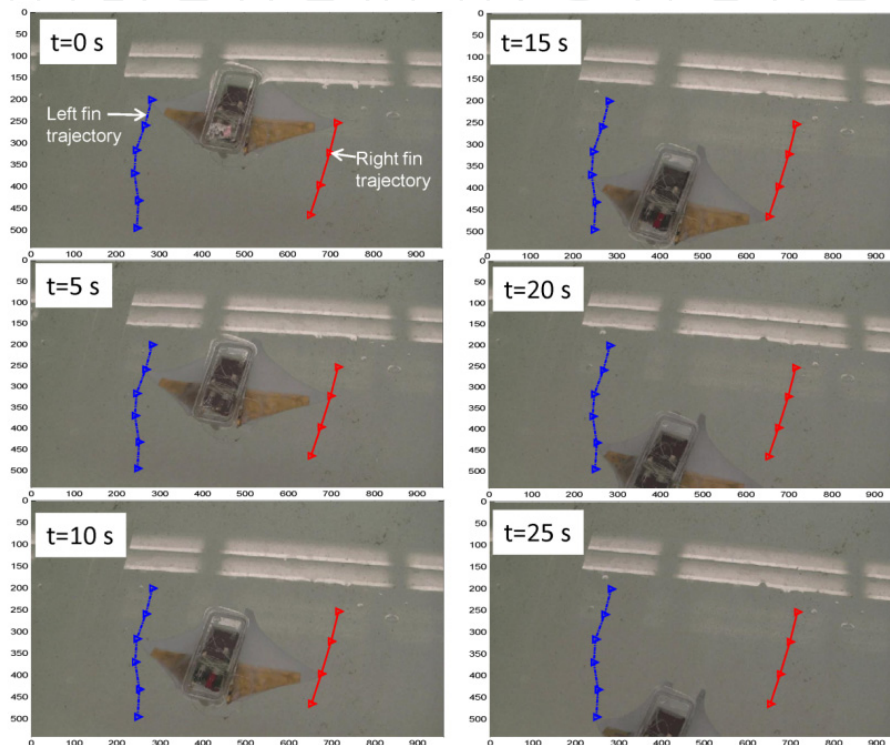


Figure 16. Snap shots of free-swimming robotic manta ray.

Each snap shot was taken every 5 seconds. A swim speed of 0.74 cm/s was calculated from the movie using the Edge Detection program in the LabVIEW. Since the body length was 11 cm, the speed in body length per second (BL/s) was 0.067.

2.4. Comparison of ray-like swimming robots

In our previous work, we developed an artificial pectoral fin that consists of four IPMCs bonded by PDMS membrane. The robot swam at 0.42 cm/s (0.053 BL/s) consuming 1 W in power. Many other research groups have been developed ray-like robots, using IPMCs, servomotors, and shape memory alloys as actuators. The comparison of ray-like swimming robots is shown in Table 1. It indicates that the IPMC powered ray-like robots are lighter and consume less power than the robots actuated by a servomotor or SMA. But they swim at lower speed for the reasons that IPMC is unable to flap at high frequency and generated force is also very low.

Reported Article	Speed (BL/s)	Power (W)	Weight (g)	Actuator
This chapter	0.067	2.5	55	IPMC
Chen et al. 2010	0.053	1	55	IPMC
Punning, et al. 2004	0.038	2.2	60	IPMC
Zhou et al, 2012	0.8	10.8	7300	Servo Motor
Wang et al, 2009	0.43	Not given	354	SMA

Table 1. Comparison of Ray-like Robots.

The advantages of using IPMCs as artificial muscle in ray-like swimming robots are: 1) low actuation voltage; 2) works well in wet conditions; 3) no gears and motors, 4) simple mechanical structure; 5) low noise; 6) able to be shaped in bio-inspired engineering design. However, IPMC can only generate low force with slow response time, which limits the swimming speed of the robot. To accommodate the disadvantages and utilize the advantages, an optimal design of the pectoral fin must be conducted, where the dimensions and location of the IPMC actuator are optimized. The challenge arises from modelling the IPMC actuating membrane to produce optimal 3D kinematic motions, which is a future focus. Another focus will be on modelling of the fluid dynamics introduced by the 3D kinematic motions of the fin, to understand how the thrust force is generated.

3. A novel buoyancy control device enabled by IPMC

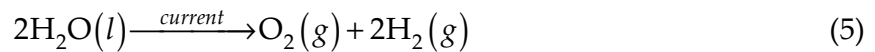
In this study, a novel depth control device has been designed and built. The proof-of-concept device utilizes the principles of electrolysis of water, enhanced by the inclusion of an ionic polymer-metal composite (IPMC) membrane as a medium. The device design incorporates an artificial bladder where the volume of gas generated by electrolysis is controlled by a solenoid valve, thus changing the device's buoyancy. A set of gold electrodes, separated by an IPMC film, is used as a lightweight and compact electrolysis generator. IPMC acts as stable, low power, highly efficient and environmentally friendly gas generator. Experimental results using open-loop control show that the device is capable of controlling its buoyancy efficiently with no noise and low power consumption. Applications for this technology include integration into bio-inspired, unmanned underwater vehicles.

3.1. Mechanism of buoyancy control

3.1.1. Gas generation by water electrolysis

When an electric current is applied between positively and negatively charged electrodes in ionized water, a chemical reaction occurs, in which pure oxygen and hydrogen gases are produced. Hydrogen gas appears at the cathode electrode (3) and oxygen gas appears at the anode electrode (4). Equation (5) shows the net reaction (Shaaban, 1994).





Two thin gold plates, each approximately 2 cm by 2 cm, are used as electrodes (Fig. 17). Typically, the two plates are placed 1-2 cm apart to allow the current to travel through the water. Most electrolysis experiments are performed in ionic solutions, which are usually prepared by adding salt, acid, or base. However, adding electrolytes is not feasible in this case because the device must be able to generate gas in regular tap water.

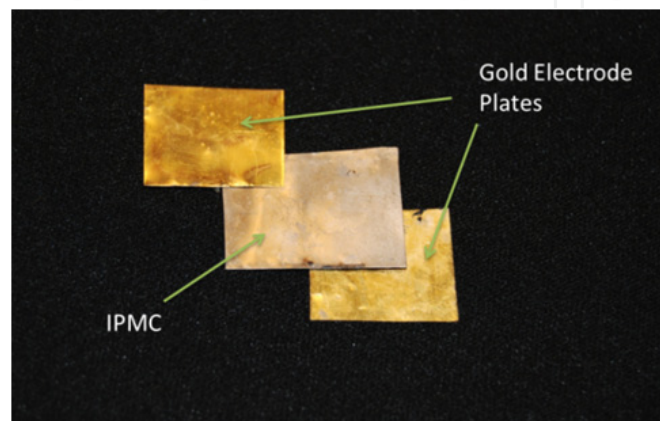


Figure 17. Gold electrodes and a sample of an ionic polymer-metal composite.

Electrolysis in tap water is much slower because of the limited number of ions present. In order to enhance the electrolysis process, an IPMC (150 μm thick) is placed directly in between the electrodes (Fig. 17). In this study, the IPMC is used only as a medium to contain electrolytes and provide channels for ion movement in the electrolysis process. By allowing the current to flow through the electrodes and IPMC, oxygen and hydrogen gases are generated. These gases are collected in a gas chamber, displacing the water in the artificial bladder. Because the gas mixture has a much lower density than that of water, the device becomes more positively buoyant. Care must be taken because the mixture contains a proportion of constituents such that it can burn instantly when ignited.

3.1.2. Gas releasing mechanism by solenoid valve

The mechanism to control the release of gas, and thereby depth, uses a two-way solenoid valve (Hargraves Tech. Corp, Part # 75M06U2.A005S). This valve is closed in its non-actuated state and is suitable for the size and power constraints of this proof-of-concept design. This particular valve can be opened by applying 6 VDC voltage and has a power consumption and mass of 0.5 W and 5 g, respectively. When the valve is actuated, the gas formed during electrolysis escapes from the device and water supersedes. As a result, the density of the device increases, causing it to become more negatively buoyant. When the valve is closed, water cannot enter through a bottom opening because the pressure inside the device is equal to that of outside. Thus the device is able to maintain the same depth by

having a constant buoyant force. In order to travel up or downwards, gas is either produced or released in a controlled manner.

3.2. Device design

The device consists of three parts: bottom chamber, middle seal, and top chamber. The overall schematic of the device is shown in Fig. 18. The parts are drawn using Autodesk Inventor 2010 and printed using a Fused Deposition Modeling (FDM) machine (uPrint Plus by Dimension). The device is approximately 15 cm tall, 6.5 cm in diameter, and has a mass of 114 g.

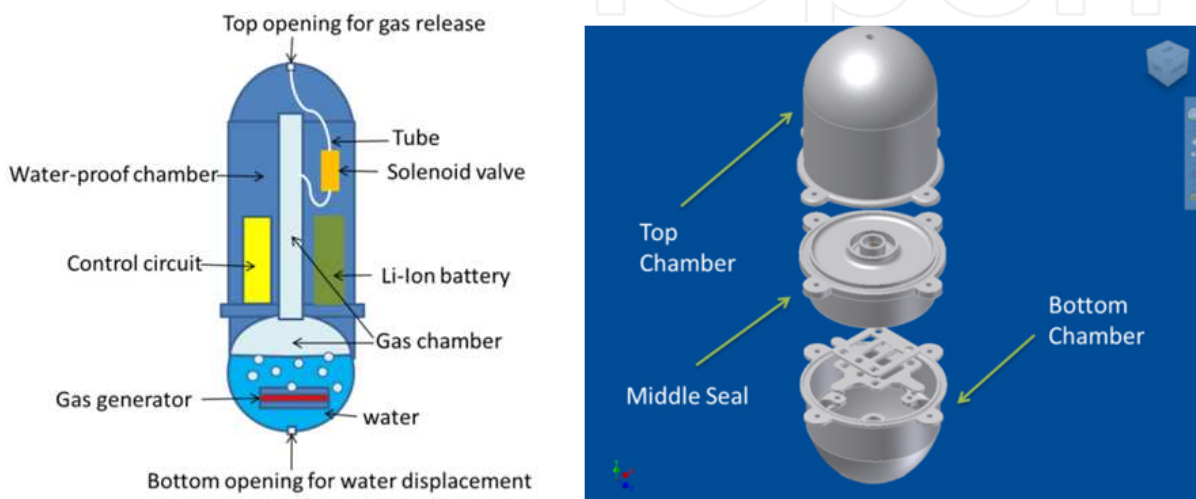


Figure 18. Schematic of the device (left); Computer drawing of the depth control device (right).

3.2.1. Bottom chamber

The bottom chamber encases the gas generator and holds water (Fig. 19). The water level varies depending on the depth location of the device. When the device is below the surface, the gas generator is submerged under water to ensure that the electrolysis can take place to allow the device to float up. The bottom chamber also has room to secure up to 8 metal washers as deadweights such that the device is initially about 80-90% submerged. On the bottom of the chamber, there is a small opening to allow water to enter or escape the device. This opening ensures that the inside and outside pressures are kept equal.

3.2.2. Middle seal

The purpose of the middle seal (Fig. 20) is to provide waterproofing of the electronics in the top chamber (Fig. 21). The bottom inner surface is concaved to direct the gas products to the gas chamber.

3.2.3. Top chamber

The top chamber is partitioned into a waterproof chamber and a gas chamber. The waterproof chamber contains all the electronics, Li-ion battery and Solenoid valve (Fig. 21).

The gas chamber contains a mixture of air and gases produced at the electrodes in the bottom chamber. A tube connects the gas chamber to the device surroundings via solenoid valve.

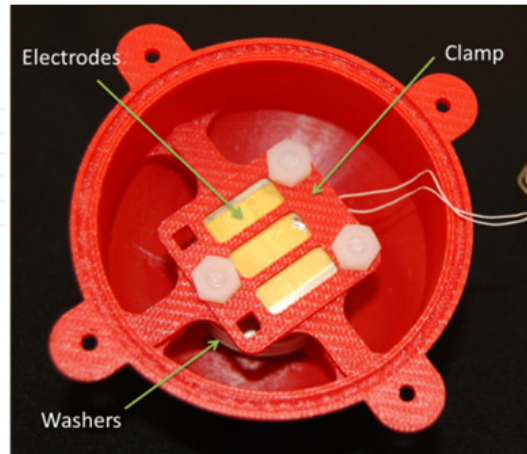


Figure 19. Bottom Chamber with electrodes assembly (Top View).

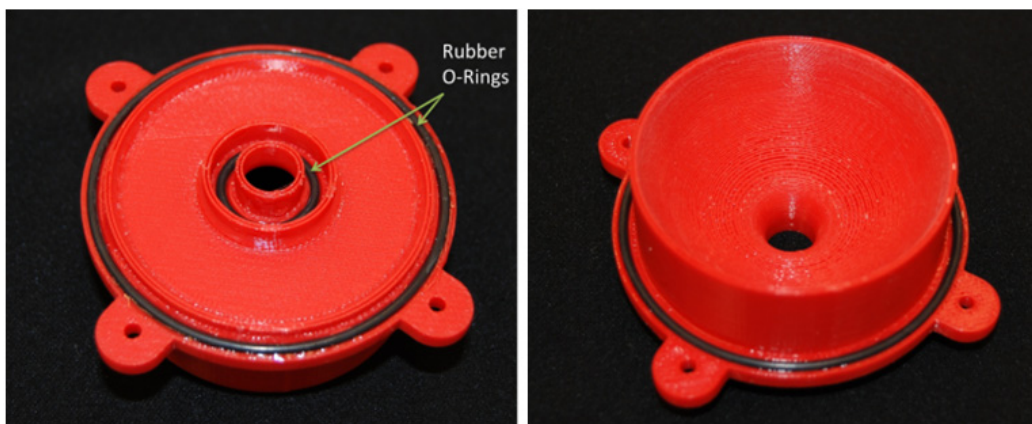


Figure 20. Middle Seal with rubber O-rings (Left: Top view; Right: Bottom view).

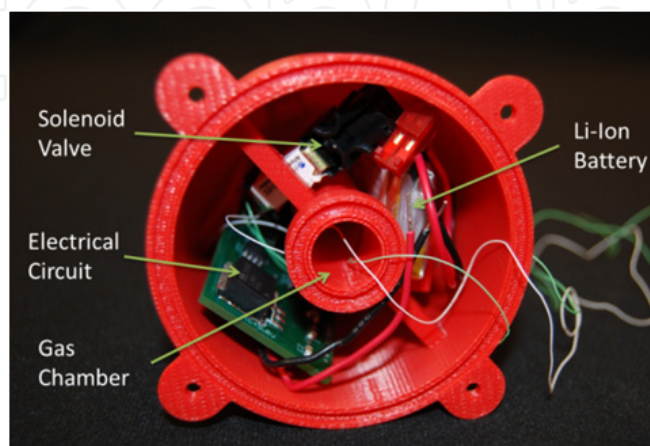


Figure 21. Top Chamber with electronic components and gas chamber.

3.2.4. On-board electrical circuit design

The on-board circuit (Fig. 22) provides actuation voltage signals to the electrodes and solenoid valve. A rechargeable 7.4 V, 400 mAh AA Portal Power Corp Lithium Ion Polymer battery is used as a power source and PIC12F508 microcontroller is used to generate two square wave control signals, S_1 and S_2 . A square wave is chosen for simplicity. Since the microcontroller draws only 25 mA, two H-bridge drivers are used to provide up to 2 A peak current output to the electrodes and solenoid valve, which draw up to 500 mA and 80 mA, respectively. Amplitude of the voltage that controls the valve, V_{p1} , is 7.4 V. A voltage regulator sets the amplitude of the voltage applied to the electrodes and microcontroller, V_{p2} , to 5 V. Mass of the circuit and the battery are 11.5 g and 19.1 g, respectively.

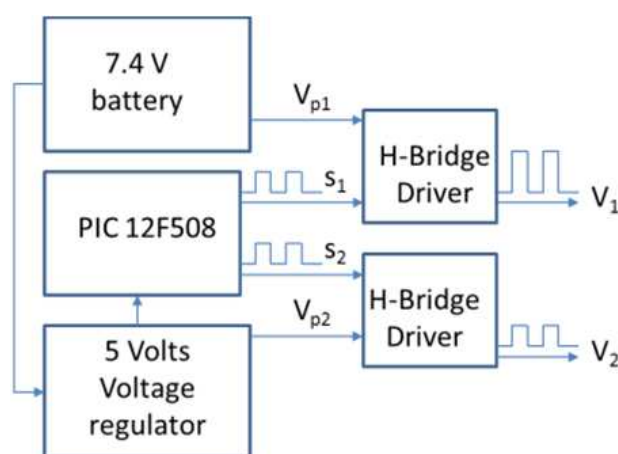


Figure 22. Circuit schematics.

3.3. Experimental results

3.3.1. Gas generation rate

An experiment is set up to measure the gas generation rate at different voltage levels. Voltages ranging from 2.0 V to 6.0 V at 0.5 V intervals are applied to the electrodes using an Agilent DC Power Supply (Model #E3646A). The hydrogen and oxygen gases generated are collected using water displacement technique with 50 mL graduated cylinder (Fig. 23(left)). A constant voltage is applied for 60 s then the average current and displaced volumes are recorded. The gas generation rate can be found by dividing the displaced volume by 60 s. Gas generation rate vs. power consumption is plotted (Fig. 23(right)) and a least squares regression line is fitted to find a correlation. The results indicate a fairly strong linear relationship between gases generated and power consumption. The proportionality constant is approximately 0.032 mL/J.

The on-board circuit is set up such that the output voltage is 5V. However the actual voltage measured across the electrodes is 4 V due to limited capacity of the battery. At this voltage, the average current and power consumption based on 5 trials are 0.3 A and 1.2 W, respectively. The average gas generation rate was 0.048 mL/s. The linear model predicts 0.040 mL/s at this power so the model and the result are in a fair agreement.

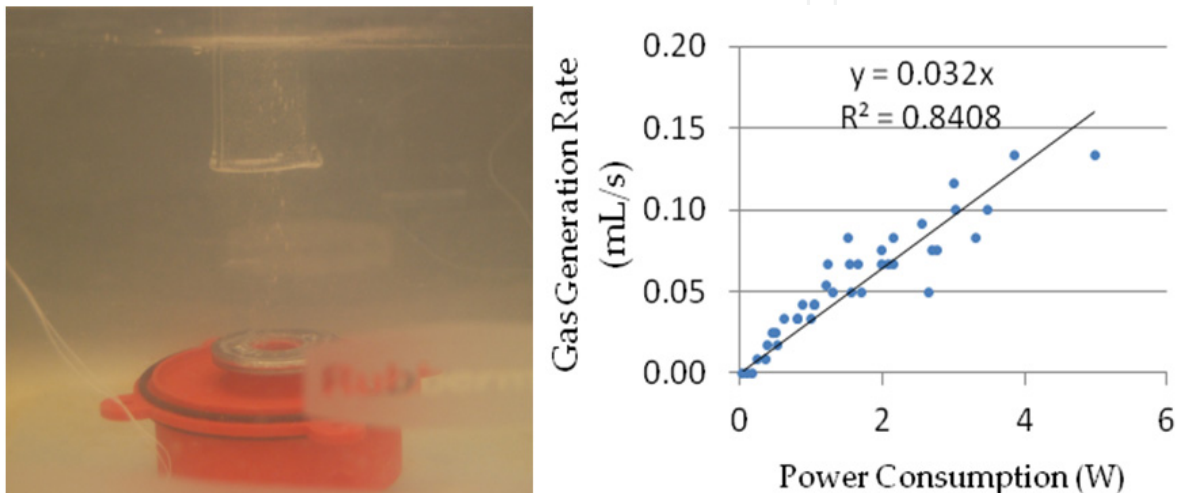


Figure 23. Gas generation rate experiment set-up; using water displacement technique to collect the gas generated (left); Gas generation rate vs. power consumption (right).

3.3.2. Diving test

The depth control device is tested in a water tank (1.5 m wide, 4.7 m long, and 0.9 m deep). The tank is filled with tap water at a room temperature. A critical mass is when the device is about 95% submerged under water, at which a slight decrease in buoyancy causes the device to sink. The critical mass of the device is experimentally found to be 283 g. Because the mass of the device is 114 g, 169 g of metal washers are added to the bottom chamber as deadweights. This mass is also equal to the payload for this particular device. The microcontroller in the circuit is programmed such that there is an initial 3-minute delay to allow time for assembly and fastening of the bolts. After the initial delay, the solenoid valve turns on for 12 s to allow gas to escape such that the device will sink to the bottom of the tank. Then the solenoid valve turns off and 5 V is applied to the electrode plates for up to 15 minutes. Gases generated by the electrolysis fill the gas chamber, which displaces the water inside the bottom chamber. Thus, the device becomes more positively

buoyant. The time it takes to rise back up to the top is measured. Fig. 24 shows the timing of the control signals.

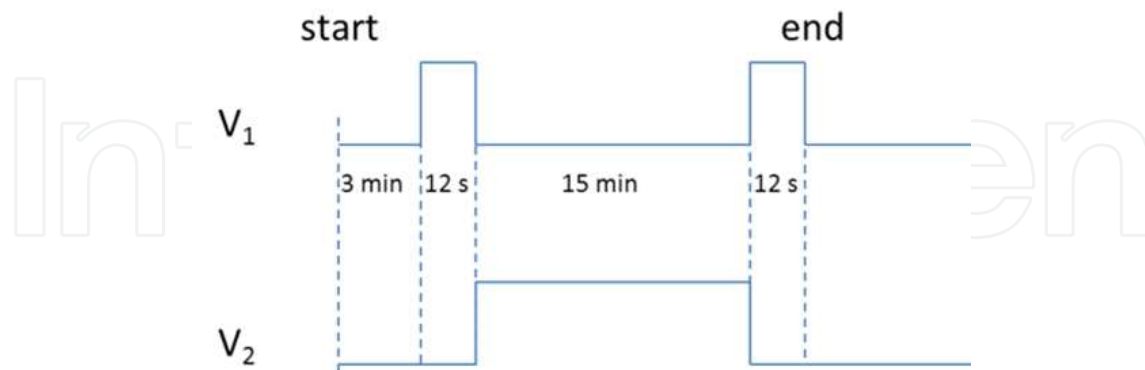


Figure 24. Timing of the control signals.

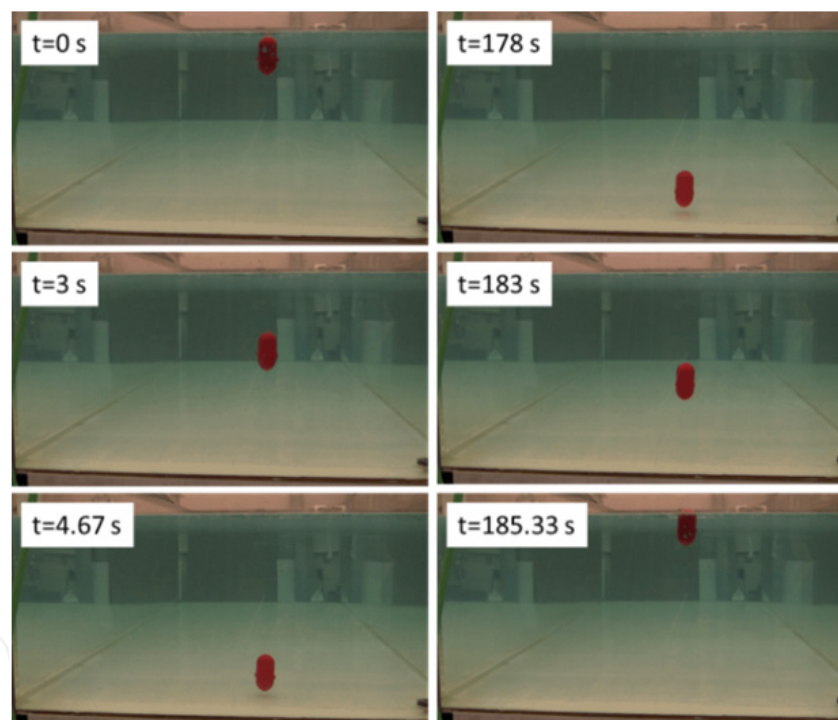


Figure 25. Snapshots of the device during open-loop testing.

It took approximately 4.7 s for the device to sink to the bottom of the tank and 180 s to rise back up to the top. The power consumption for sinking and rising are 0.5 W and 1.2 W, respectively. Fig. 25 shows snapshots of a successful demonstration of the open-loop proof-of-concept depth control device. In order to reduce the rising response time, multiple sets of electrodes can be implemented and actuated simultaneously at a higher voltage. To decrease the current rising time by a factor of 1/3 (60 s), a gas generation rate must triple to be at least 0.14 mL/s. This is achievable with two sets of electrodes with approximately 6 V actuation voltages.

3.3.3. Discussion

The advantages of using IPMC as electrolysis generator in depth control device are: 1) quiet gas generation; 2) low activation voltage; 3) compact design. The challenge arises from the low gas generation rate. In the close-loop depth control (Chen et al, 2012b), a fast gas generation rate is required to compensate the depth drop caused by disturbances and the volume decrease caused by water pressure, rapidly. A multi-IPMC electrodes design might be a good solution to increase the gas generation. However, it also increases the power consumption. In our future work, an additional volume-fixed gas storage chamber will be used to collect the generated gas with high pressure. Another solenoid valve will be used to release the high pressure gas into the gas chamber, which controls the volume of the device rapidly. One may be aware of hydrogen and oxygen explosive gas in the gas storage chamber. A two-gas-chamber design can solve this issue by separating oxygen and hydrogen gases. If a fuel cell is embedded, these gases can be recycled as fuel to recharge the battery, which makes the depth control more power efficient.

4. Chapter conclusion

In this Chapter, we presented two studies on IPMC artificial muscles in bio-inspired engineering research. In the first study, we developed a bio-inspired robotic manta ray powered by IPMC pectoral fin. We developed a novel synthesis process to fabricate IPMC pectoral fin that is capable of 3D kinematic motion and characterized the pectoral fin in terms of tip deflection (up to 100%), bode plot (0.4 Hz cut-off frequency), twist angle (up to 40°), and power consumption (below 1.5 W). A small size free-swimming robotic manta ray has been developed and experimental results have demonstrated its free-swimming capability with speed at 0.067 body length per second and 2.5 W power consumption. In the second study, we developed a novel buoyancy control device as an artificial swimming bladder. IPMC acted as an efficient, environmentally friendly water electrolysis generator to gain volume of the device while a solenoid valve was used as gas releasing controller. A compact and low power device has been assembled with an on-board open loop controller. Experimental results have shown that the device was able to control its 0.9 m depth within 3 minutes.

In both studies, advantages and challenges of IPMC in bio-inspired engineering research have been addressed. In this first study, the advantages of using IPMC as artificial muscle are: 1) low actuation voltage; 2) working well in wet condition; 3) low noise; 4) simple mechanical structure; 5) able to be shaped into bio-inspired engineering design. The disadvantages are: 1) low generated force; 2) slow response time. The challenge in this study comes from optimal design of the pectoral fin. In future research, we will focus on modeling an IPMC powered pectoral fin and modeling of the fluid dynamics introduced by the 3D kinematic motions of the fin. In the second study, the advantages of using IPMC as electrolysis generator are: 1) low noise; 2) compact design; 3) low

activation voltage and low power consumption. The disadvantage arises from 1) slow gas generation rate that limits its capability of feedback depth control; 2) unstable nonlinear dynamics. The challenge in this study is feedback depth control that requires high gas generation rates and complex nonlinear control algorithms. In future work, we will focus on nonlinear feedback control and improved device design that can gain gas volume rapidly.

Author details

Zheng Chen, T. Um and Hilary Bart-Smith*
University of Virginia, USA

Acknowledgement

This research was supported in part by the Office of Naval Research (ONR) under the Multidisciplinary University Research Initiative (MURI) Grant N00014-08-1-0642 and the David and Lucille Packard Foundation.

5. References

- Bar-Cohen, Y. (2004). Electric flex. *IEEE Spectrum*, Vol.41, No.6, pp. 29-33, ISSN 0018-9235
- Bar-Cohen, Y. (2000). Electroactive Polymers as Artificial Muscles - Capabilities, Potentials and Challenges, In: *Handbook on Biomimetics*, Y. Osada, (Ed.), 936-950, NTS Inc.
- Bond, C. (1996). Swim Bladder. In: *Biology of Fishes* (2nd edition). pp. 283-290, Saunders College Publishing.
- Chen, Z. & Tan, X. (2008). A Control-oriented and Physics-based Model for Ionic Polymer-Metal Composite Actuators. *IEEE/ASME Transactions on Mechatronics*, Vol. 13, No. 5, pp. 519-529, ISSN 1083-4435.
- Chen, Z. ; Shatara, S. & Tan, X. (2010). Modeling of Biomimetic Robotic Fish Propelled by an Ionic Polymer-Metal Composite Caudal Fin. *IEEE/ASME Transactions on Mechatronics*, Vol. 15, No. 3, pp. 448-459, ISSN 1083-4435.
- Chen, Z & Tan, X. (2010). Monolithic Fabrication of Ionic Polymer-Metal Composite Actuators Capable of Complex Deformation, *Sensors and Actuators A: Physical*, Vol. 157, No. 2, pp. 246-257, ISSN 0924-4247.
- Chen, Z.; Um, T. I. & Bart-Smith, H. (2011). A Novel Fabrication of Ionic Polymer-Metal Composite Membrane Actuator Capable of 3-dimensional Kinematic Motions. *Sensors and Actuators A: Physical*, Vol. 168, No. 1, pp. 131-139, ISSN 0924-4247.
- Chen, Z.; Um, T. I. & Bart-Smith, H. (2012a). Bio-inspired Robotic Manta Ray Powered by Ionic Polymer-Metal Composite Artificial Muscles. *International Journal of Smart and Nano Materials*, to appear, ISSN 1947-5411.

* Corresponding Author

- Chen, Z; Um, T. I. & Bart-Smith, H. (2012b). Modelling and Control of Artificial Bladder Enabled by Ionic Polymer-Metal Composite. *Proceedings of the 2012 American Control Conference*, to appear, June 27-29 2012, Montreal, Canada, 2012, pp. 3340-3345.
- Chung, C.; Fung, P.; Hong, Y.; Ju, M.; Lin, C. & Wu, T. (2006). A Novel Fabrication of Ionic Polymer-Metal Composites (IPMC) Actuator with Silver Nano-powders. *Sensors and Actuators B: Chemical*, Vol. 117, No. 2, pp. 367–375, ISSN 0925-4005.
- Gao, J.; Bi, S.; Xu, Y. & Liu, C. (2007). Development and Design of A Robotic Manta Ray Featuring Flexible Pectoral Fins. *Proceedings of the 2007 IEEE International Conference on Robotic and Biomimetics*, pp. 519-523, ISBN 978-1-4244-1761-2, Sanya, China, December 15-18, 2007.
- Guo, S.; Fukuda, T. & Asaka, K. (2003). A New Type of Fish-like Underwater Microrobot. *IEEE/ASME Transactions on Mechatronics*, Vol. 8, No. 1, pp. 136–141, ISSN 1083-4435.
- Kim, K. J. & Shahinpoor, M. (2002). A Novel Method of Manufacturing Three-dimensional Ionic Polymer-Metal Composites (IPMCs) Biomimetic Sensors, Actuators, and Artificial Muscles. *Polymer*, Vol. 43, No. 3, pp. 797–802, ISSN 0032-3861.
- Kim, K. J. & Shahinpoor, M. (2003). Ionic polymer-metal composites: II. Manufacturing techniques. *Smart Materials and Structures*, Vol. 12, No. 1, pp. 65–79, ISSN 0964-1726.
- Kim, K. J.; Pugal, D. & Leang, K. K. (2011). A Twistable Ionic Polymer-Metal Composite Artificial Muscle for Marine Applications. *Marine Technology Society Journal*, Vol. 45, No. 4, pp. 83-98, ISSN 0025-3324.
- Kim, S. J.; Lee, I. T. & Kim. Y. H. (2007). Performance Enhancement of IPMC Actuator by Plasma Surface Treatment. *Smart Materials and Structures*, Vol. 16, No. 1, pp. N6–N11, ISSN 0964-1726.
- Lee, S. J.; Han, M. J.; Kim, S. J.; Jho, J. Y.; Lee, H. Y. & Kim, Y. H. (2006). A New Fabrication Method for IPMC Actuators and Application to Artificial Fingers. *Smart Materials and Structures*, Vol. 15, No. 5, pp. 1217–1224, ISSN 0964-1726.
- Lin, L.; Xu, H.; Xie, H. & Shen, L. (2010). Bionic Bladder Based Depth Control for Bionic Underwater Robots. *Proceedings of 2010 8th IEEE International Conference on Control and Automation*, pp. 932-936, ISBN 978-1-4244-5195-1, June 9-11, Xiamen, China, 2010.
- McFarland, D.; Gihespy, I. & Honary, E. (2003). Divebot: A Diving Robot with A Whale-like Buoyancy Mechanism. *Robotica*, Vol. 21, No. 4, pp. 385-398, ISSN 0263-5747
- Millet, P.; Pineri, M. & Durand, R. (1989). New Solid Polymer Electrolyte Composites for Water Electrolysis. *Journal of Applied Electrochemistry*, Vol. 19, No. 2, pp. 162-166, ISSN 0021-891X.
- Mojarrad, M. & Shahinpoor, M. (1996). Noiseless Propulsion for Swimming Robotic Structures Using Polyelectrolyte Ion-exchange Membranes. *Proceedings of SPIE Conference on Smart Structures and Materials*, Vol. 2176, pp. 183, ISSN 0277-786X, February 26, San Diego, California, 1996.
- Moored, K.; Smith, W.; Hester, J.; Chang, W. & Bart-Smith, H. (2008). Investigating the Thrust Production of A Myliobatoid-inspired Oscillating Wing. *Advances in Science and Technology*, Vol. 58, pp. 25–30, ISSN 1662-0356.

- Moored, K. & Bart-Smith, H. (2009). Investigation of Clustered Actuation in Tensegrity Structures. *International Journal of Solids and Structures*, Vol. 46, No. 17, pp. 3272–3281, ISSN 0020-7683.
- Nemat-Nasser, S. & Li, J. (2000). Electromechanical Response of Ionic Polymer–Metal Composites. *Journal of Applied Physics*, Vol. 87, No. 7, pp. 3321–3331, ISSN 0021-8979.
- Nemat-Nasser, S. (2002). Micromechanics of Actuation of Ionic Polymer–Metal Composites. *Journal of Applied Physics*, Vol. 92, No. 5, pp. 2899–2915, ISSN 0021-8979.
- Punning, A.; Anton, M.; Kruusmaa, M. & Aabloo, A. (2004). A Biologically Inspired Ray-like Underwater Robot with Electroactive Polymer Pectoral Fins. *Proceedings of the IEEE International Conference on Mechatronics and Robotics 2004*, pp. 241-245, ISBN 3-938153-50-X, September 13-15, Aachen, Germany, 2004.
- Rosenberger, L. J. (2001). Pectoral Fin Locomotion in Batoid Fishes: Undulation versus Oscillation. *The Journal of Experimental Biology*, Vol. 204, pp. 379–394, ISSN 0022-0949.
- Shahinpoor, M. (1992). Conceptual Design, Kinematics and Dynamics of Swimming Robotic Structures Using Ionic Polymeric Muscles. *Smart Materials and Structures*, Vol. 1, No. 1, pp. 91-94, ISSN 0964-1726.
- Shahinpoor, M. & Kim, K. J. (2001). Ionic polymer-metal composites: I. Fundamentals. *Smart Materials and Structures*, Vol. 10, No. 4, pp. 819–833, ISSN 0964-1726.
- Shahinpoor, M.; Kim, K. J. & Leo, D. (2003). Ionic Polymer-Metal Composites as Multifunctional Materials. *Polymer Composites*, Vol. 24, No. 1, pp. 24-33, ISSN 0272-8397
- Shahinpoor, M & Kim K. J. (2005). Ionic polymer–metal composites: IV. Industrial and medical applications. *Smart Materials and Structures*, Vol. 14, No. 1, pp. 197–214 ISSN 0964-1726.
- Shaaban, A. H. (1994). Pulsed DC and Anode Depolarization in Water Electrolysis for Hydrogen Generation. In: *StormingMedia*, 01.08.1994, Available from <http://www.stormingmedia.com>.
- Shimizu, N.; Hotta, S.; Seekiya, T. & Oda, O. (2005). A Novel Method of Hydrogen Generation by Water Electrolysis Using an Ultra-short-pulse Power Supply. *Journal of Applied Electrochemistry*, Vol. 36, No. 4, pp. 419-423, ISSN 0021-891X.
- Tan, X.; Kim, D.; Usher, N.; Laboy, D.; Jackson, J.; Kapetanovic, A.; Rapai, J.; Sabadus, B. & Zhou, X. (2006). An Autonomous Robotic Fish for Mobile Sensing. *Proceedings of the 2006 IEEE/RSJ International Conference on Intelligent Robots and Systems*, pp. 5424-5429, ISBN 1-4244-0259-X, Oct. 9-15, Beijing, China, 2006.
- Um, T. I.; Chen, Z. & Bart-Smith, H. (2011). A Novel Electroactive Polymer Depth Control Device for Bio-inspired Underwater Vehicles. *Proceedings of the IEEE International Conference on Robotics and Automation*, pp. 172-177, ISBN 978-1-61284-380-3, May 13-19, Shanghai, China, 2011.
- Wang, Z.; Wang, Y.; Li, J. & Hang, G. (2009). A Micro Biomimetic Manta Ray Robot Fish Actuated by SMA. *Proceedings of the 2009 IEEE International Conference on Robotics and Biomimetics*, pp. 1809-1813, ISBN 978-1-4244-4774-9, Guilin, China, December 19-25, 2009.

Zhou, C. & Low, K. H. (2102). Design and Locomotion Control of A Biomimetic Underwater Vehicle with Fin Propulsion. *IEEE/ASME Transactions on Mechatronics*, Vol. 17, No. 1, pp. 25-35, ISSN 1083-4435.

IntechOpen

IntechOpen